Molecular modeling of hydrogen bonding fluids: Vapor-liquid coexistence and interfacial properties

Martin Horsch[1], Martina Heitzig[2], Thorsten Merker[3], Thorsten Schnabel[2], Yow-Lin Huang[1], Hans Hasse[3], and Jadran Vrabec[1]

[1] Lehrstuhl für Thermodynamik und Energietechnik (ThEt), Universität Paderborn, Warburger Str. 100, 33098 Paderborn, Germany[†]
[2] Institut für Technische Thermodynamik und Thermische Verfahrenstechnik (ITT), Universität Stuttgart, Pfaffenwaldring 9, 70569 Stuttgart, Germany
[3] Lehrstuhl für Thermodynamik (LTD), Technische Universität Kaiserslautern, Erwin-Schrödinger-Str. 44, 67663 Kaiserslautern, Germany

1 Introduction

A major challenge for molecular modeling consists in the definition of unlike interaction potentials. A variety of combination rules were proposed in the past. In a broad study on fluid mixtures [1], it was recently shown that none of them is clearly superior and that all are suboptimal in many cases when accurate predictions of properties like the mixture vapor pressure are needed. The well known Lorentz-Berthelot rule performs quite well and can be used as a starting point. If more accurate results are required, it is often advisable to adjust the dispersive interaction energy parameter which leads to very favorable results [1, 2, 3, 4, 5].

A similar approach should be followed for effective pair potentials acting between fluid particles and the atoms of a solid wall, which can only be reliable if fluid-wall contact effects are taken into account, e.g., by fitting model parameters to adsorption isotherms [6]. The present study continues the line of research suggested by Werder *et al.* [7] who adjusted unlike parameters to data on the contact angle formed between the wall and a vapor-liquid interface. Teletzke *et al.* [8] used DFT based methods to examine the dependence of wetting and dewetting transitions on characteristic size and energy parameters of the fluid-wall dispersive interaction. MD simulation can be applied for the same purpose, leading to a consistent molecular approach.

On the molecular level, the precise position of the vapor-liquid phase boundary is defined by a cluster criterion. Many different criteria are known and it is not immediately obvious which of them leads to the most accurate results [9]. In nanoscopic systems, minute absolute differences can lead to comparably large relative devia-

[†] Author to whom correspondence should be addressed: Prof. Dr.-Ing. habil. J. Vrabec. E-mail: jadran.vrabec@upb.de.

tions. Therefore, the viability of several criteria is compared in the present study with the purpose of excluding errors due to an inaccurate detection of the interface.

If the cohesion of the liquid phase is partly due to hydrogen bonds, successful molecular models for pure fluids can often be developed on the basis of an *ab initio* study of the charge distribution as well as the equilibrium position of the nuclei. This sterically realistic approach, combined with adjusting the Lennard-Jones (LJ) potential parameters to vapor-liquid equilibrium (VLE) data, leads to empirical models that correctly reproduce and predict thermophysical fluid properties over a wide range of conditions [10]. The present work applies this approach to mixtures containing hydrogen bonding components. Often potential parameters determined for one fluid carry over to a derivative with different substituents, opening the possibility of creating generic molecular models. Such a model is presented for benzyl alcohol.

The following publications in peer-reviewed international journals contribute to the present project:

- Schnabel, T., Vrabec, J. & Hasse, H. Molecular simulation study of hydrogen bonding mixtures and new molecular models for mono- and dimethylamine. *Fluid Phase Equilib.* **263**: 144–159 (2008).
- Eckl, B., Vrabec, J. & Hasse, H. An optimized molecular model for ammonia. *Mol. Phys.* **106**: 1039–1046 (2008).
- Eckl, B., Vrabec, J. & Hasse, H. Set of molecular models based on quantum mechanical ab initio calculations and thermodynamic data. *J. Phys. Chem. B* **112**: 12710–12721 (2008).
- Vrabec, J., Huang, Y.-L. & Hasse, H. Molecular models for 267 binary mixtures validated by vapor-liquid equilibria: a systematic approach. In press.
- Huang, Y.-L., Vrabec, J. & Hasse, H. Prediction of ternary vapor-liquid equilibria for 33 systems by molecular simulation. Submitted.
- Horsch, M., Heitzig, M., Dan, C., Harting, J., Hasse, H. & Vrabec, J. Contact angle dependence on the fluid wall dispersive energy. In preparation.

It would exceed the scope of the present report to give a full exposition of these articles. Instead, a few points are emphasized and arranged as follows: Firstly, mixture properties are explored for binary systems containing hydrogen bonding components. Secondly, vapor-liquid interface cluster criteria and contact angles are discussed and remarks on computational details are given. Finally, a sterically accurate generic model for benzyl alcohol is introduced and evaluated.

2 Fluid mixtures with hydrogen bonding components

Vapor-liquid equilibria of 31 binary mixtures consisting of one hydrogen-bonding and one non-hydrogen bonding component were studied. All models are of the rigid united-atom multi-center Lennard-Jones type with superimposed electrostatic sites in which hydrogen bonding is described by partial charges. The hydrogen bonding components of the studied binary mixtures are: monomethylamine (MMA) and

dimethylamine (DMA), methanol, ethanol and formic acid. The non-hydrogen bonding components are: neon, argon, krypton, xenon, methane, oxygen, nitrogen, carbon dioxide, ethyne, ethene, ethane, propylene, carbon monoxide, diflourodichloromethane (R12), tetraflouromethane (R14), diflourochloromethane (R22), diflouromethane (R32), 1,1,1,2-tetraflouroethane (R134a) and 1,1-diflouroethane (R152a).

To obtain a quantitative description of the mixture vapor-liquid equilibria, one state independent binary interaction parameter was adjusted to one experimental data point of either the vapor pressure or the Henry's law constant. Throughout, excellent predictions were found at other state points, i.e., at other compositions or temperatures as well as for the Henry's law constant, if it was adjusted to the vapor pressure, or vice versa. Figures 1 and 2 show methane + methanol as a typical example.
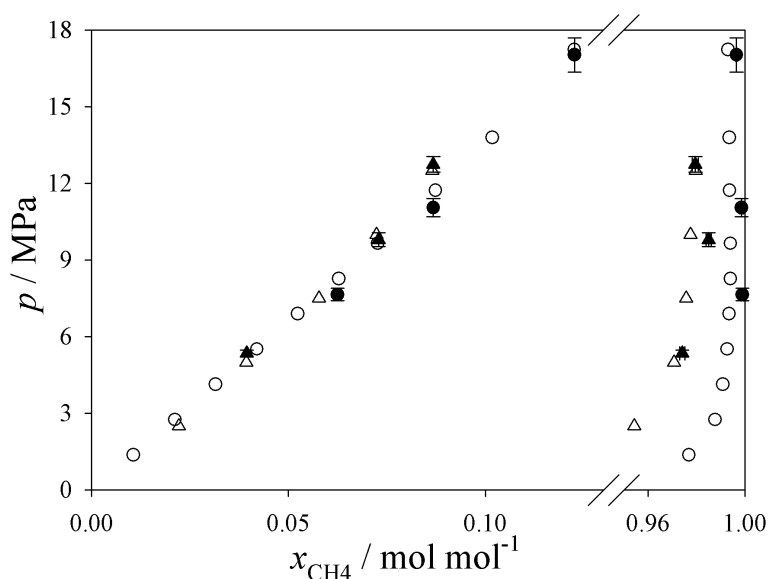

Fig. 1. Simulation data and vapor-liquid equilibria of methanol + methane: simulation data (•) and experimental data (○) at 310 K [11]; simulation data (▲) and experimental data (△) at 338.15 K [12].

Furthermore, for a set of 78 pure substances from prior work was taken to systematically describe all 267 binary mixtures of these components for which relevant experimental VLE data is available. Again, per binary system, one state independent binary interaction parameter in the energy term was adjusted to a single experimental vapor pressure. The unlike energy parameter was thereby altered usually by less than 5 % from the Berthelot rule. The mixture models were validated regarding the vapor pressure at other state points and also regarding the dew point composition, which is a fully predictive property in this context. In almost all cases, i.e. 97 %, the molecular models give excellent predictions of the mixture properties. Compared to
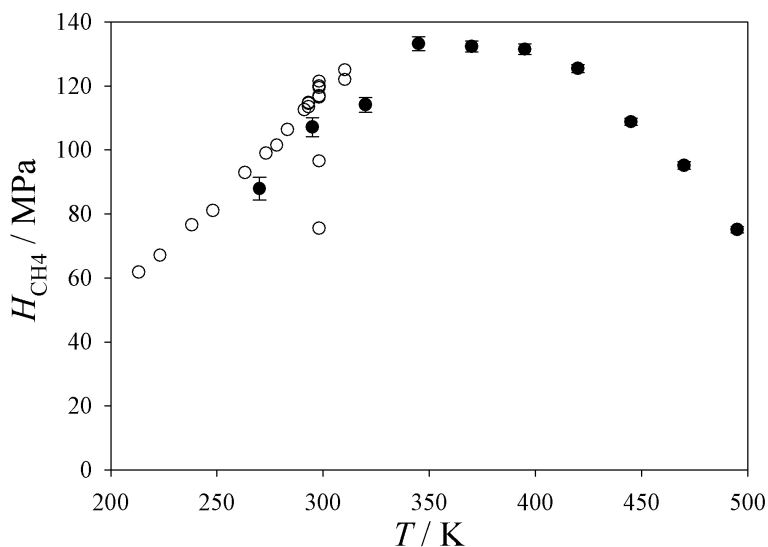
Fig. 2. Henry's law constant of methane in methanol: simulation data (●) and experimental data [13, 14, 15, 16, 17, 18, 19, 20, 21, 22] (○).

other works in the literature, this is by far the largest investigation in this direction which was facilitated by the extensive computing equipment at the High Performance Computing Center Stuttgart.

In the next step, all 33 ternary mixtures of these 78 components for which experimental VLE data is available were studied by molecular simulation. No adjustment to ternary data was carried out at all so that the calculations were strictly predictive. By comparing to experimental data, it was found that these predictions are very reliable as there was practically always an excellent match. As an example, Fig. 3 shows the ternary system consisting of methane, ethane, and carbon dioxide. Again, the computational effort was substantial, publications in the literature by other groups in this field typically cover one to two mixtures only.

3 Vapor-liquid interface cluster criteria

A suitable cluster criterion should achieve two goals: on the one hand, it needs to distinguish the bulk liquid and the bulk vapor successfully in every case – even when the vapor is supersaturated, such as in the vicinity of a droplet, or the liquid is undersaturated, such as in the vicinity of a bubble. On the other hand, the cluster criterion should also minimize noise fluctuations of the detected clusters to emphasize the signal.

The following criteria for carbon dioxide were compared for this purpose with the ls1/mardyn program [24] using a rigid two-center LJ plus point quadrupole (2CLJQ) model [25]:
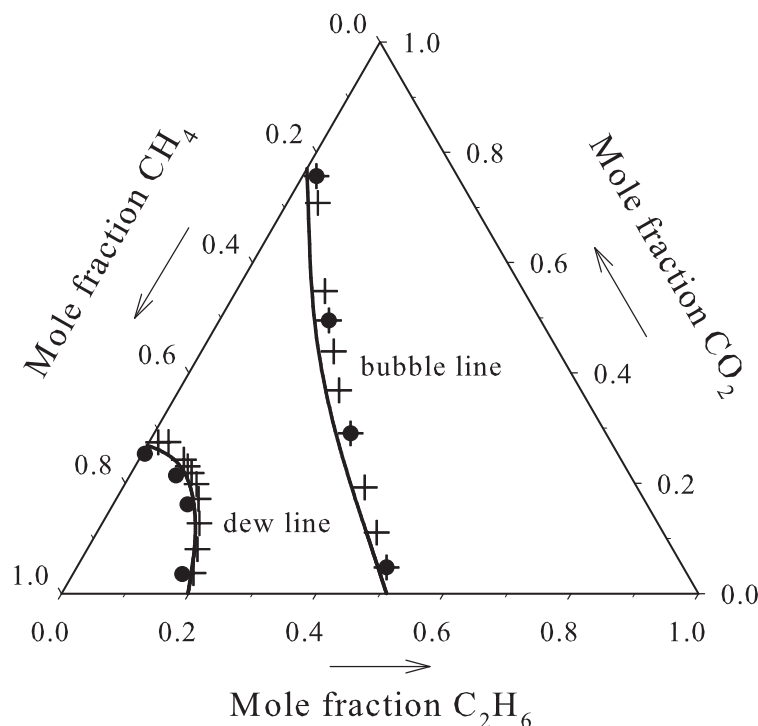
Fig. 3. Ternary vapor-liquid equilibrium phase diagram for the mixture $CH_4 + CO_2 + C_2H_6$ at 230 K and 4650 kPa: simulation data ($\bullet$), experimental data (+) of Knapp *et al.* [23], and Peng-Robinson equation of state (—).

- Stillinger [26]: all molecules with a distance of r_{St} or less from each other are liquid and belong to the same cluster (i.e., the same liquid phase or the same droplet). The Stillinger radius was set to $r_{St} = 5.7$ Å for the present simulations.
- Ten Wolde and Frenkel [27]: all molecules with at least four neighbors within a distance of r_{St} belong to the liquid. They belong to the same cluster as all other liquid molecules within a distance of r_{St}.
- Arithmetic mean, k neighbors: a molecule is liquid if the density in the sphere containing its k nearest neighbors exceeds $(\rho' + \rho'')/2$, where ρ' amd ρ'' are the saturated liquid and vapor density, respectively. The molecule belongs to the same cluster as all other liquid molecules within the radius r_k, which defines a sphere with the volume occupied by $k + 1$ molecules at a density of $(\rho' + \rho'')/2$.
- Geometric mean, k neighbors: analogous, with a density threshold of $(\rho'\rho'')^{1/2}$.

Figure 4 shows that all of the discussed criteria are applicable. The Stillinger criterion and the geometric mean density criterion with two neighbors lead to the best

results. It should be noted that at high temperatures, i.e., near the critical point, the Stillinger criterion becomes less reliable in distinguishing the liquid from a supersaturated vapor than the geometric mean density criterion.

4 Contact angle dependence on the fluid-wall interaction

In cases where no hydrogen bonds are formed between the wall and the fluid, vapor-solid and liquid-solid interfacial properties mainly depend on the fluid-wall dispersive interaction, even for hydrogen bonding fluids. Like the original LJ potential, the truncated and shifted LJ (TSLJ) model [28] accurately reproduces the dispersive interaction, if adequate values for the size and energy parameters σ and ε are specified. Due to the relatively small cutoff radius, molecular simulation based on the TSLJ fluid is comparably fast, while the full descriptive power of the Lennard-Jones potential is retained even for systems with phase boundaries [29].

In the present study, the TSLJ fluid was considered with the parameters for methane, $\sigma = 3.7241$ Å and $\varepsilon/k = 175.06$ K [29], and the wall was modeled as a system of coupled harmonic oscillators with different spring constants for transverse and longitudinal motion. The parameters of the wall model were adjusted to the C–C radial distribution function of graphite, obtained from simulations with the
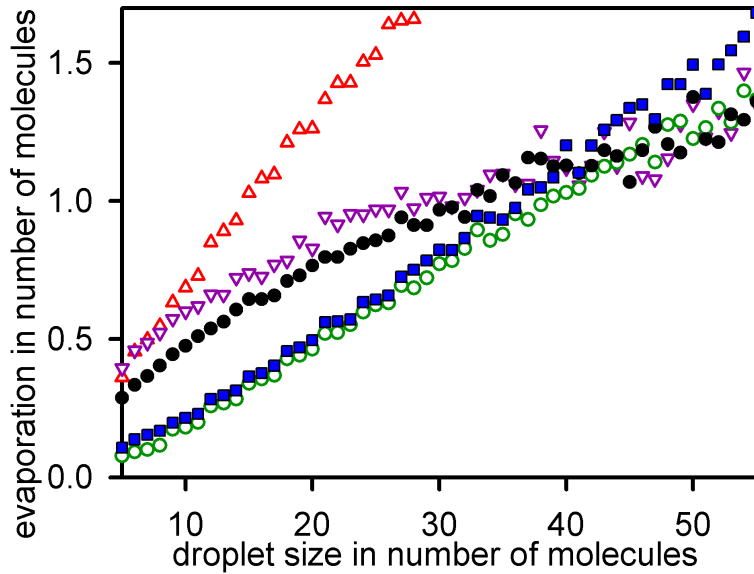

Fig. 4. Average number of molecules evaporating during a detection interval of 30 fs from droplets in a supersaturated vapor of carbon dioxide with $T = 237$ K, $\rho = 1.98$ mol/l, and $N = 1,050,000$, determined according to various cluster criteria: Stillinger ($\circ$), ten Wolde and Frenkel ($\bullet$), arithmetic mean with two ($\triangle$) and eight neighbors (∇) as well as geometric mean with two neighbors ($\square$).

Tersoff potential [30]. This distribution was rescaled because, as shown by Kelires [31], the Tersoff potential deviates by about 3 % from the actual C–C bond length in graphite. The fluid-wall interaction can be represented by the full [7] or modified [32] Lennard-Jones-12-6 potential. Following this approach, the TSLJ potential with the size parameter $\sigma_{fw} = \sigma$ as well as the energy parameter

$$\varepsilon_{fw} = W\varepsilon, \tag{1}$$

was applied for the unlike interaction between the fluid particles and the carbon atoms of the wall, with the same cutoff radius as for the fluid.

The simulations were conducted using the ls1/mardyn program with an integration time step of 1 fs. Vapor and liquid were independently equilibrated in homogeneous simulations for 10 ps. This was followed by 200 ps of equilibration for the combined system, i.e., a liquid meniscus surrounded by vapor, with a graphite wall consisting of four to seven layers, cf. Fig. 5. The periodic boundary condition was applied to the system, leaving a channel for the fluid with a height of 27 σ between the wall and its periodic image, and the contact angle was determined by averaging the density profile of the fluid via binning over at least 800 ps after equilibration. Menisci between solid walls were simulated for a reduced fluid-wall dispersive en-
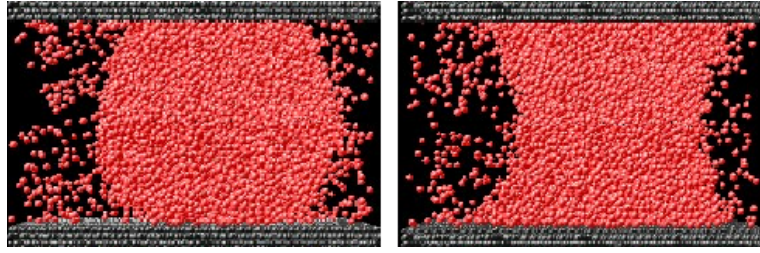

Fig. 5. Simulation snapshots for the reduced fluid-wall dispersive energy W of 0.07 (left) and 0.13 (right) at a temperature of 0.88 ε/k.

ergy W between 0.07 and 0.16 at temperatures of 0.73, 0.88, and 1 ε/k. Note that the triple point temperature of the TSLJ fluid is about 0.65 ε/k while the critical temperature is $T_c = 1.0779\ \varepsilon/k$ so that the entire regime of vapor-liquid coexistence is covered [29].

High values of W correspond to a strong attraction between fluid particles and wall atoms, leading to a contact angle $\vartheta < 90°$, i.e., to partial ($\vartheta > 0°$) or full ($\vartheta = 0°$) wetting of the surface. As expected, with increasing fluid-wall dispersive energy, the extent of wetting grows, cf. Fig. 5. As can be seen in Fig. 6, the transition from obtuse to acute contact angles occurs at W values between 0.10 and 0.13 over the whole studied temperature range. Furthermore, the symmetry relation

$$\cos\vartheta(T, W_0 - \Delta W) = -\cos\vartheta(T, W_0 + \Delta W), \tag{2}$$
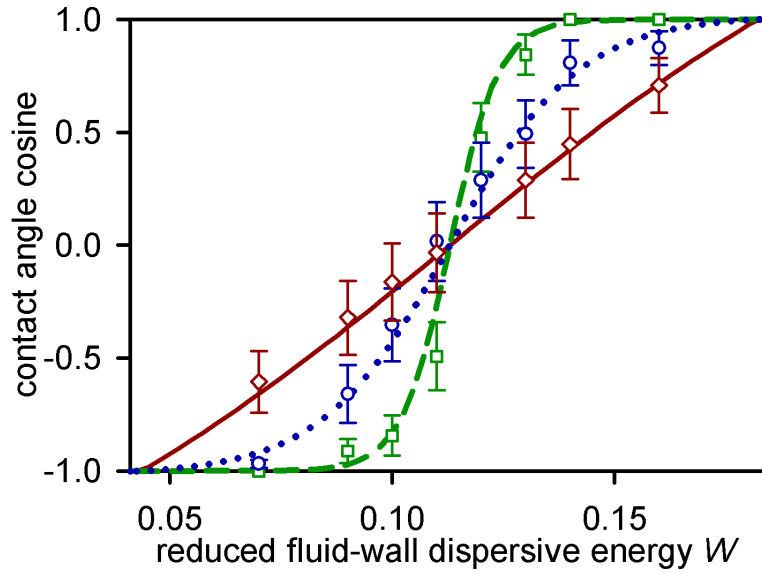
Fig. 6. Simulation results and correlation for the contact angle in dependence of the reduced fluid-wall dispersive energy W at temperatures of 0.73 (diamonds and solid line), 0.88 (circles and dotted line) as well as 1 ε/k (squares and dashed line).

is strongly suggested by the simulation results and a correlation yields a temperature independent value of $W_0 = 0.113$ for the magnitude of the reduced fluid-wall dispersive energy corresponding to $\vartheta = 90°$.

Remarkably, Teletzke *et al.* obtained a *d-W*-diagram, Fig. 5 of their work [8], describing the behavior of the contact angle with increasing T as qualitatively asymmetric with respect to W, directly contradicting Eq. (2). A direct comparison with their study, wherein both the size parameter $d = \sigma_{fw}/\sigma$ and the reduced fluid-wall dispersive energy W were varied, is impossible, however, because Teletzke *et al.* assumed an exponential decay of the interaction.

Figure 6 also shows that there is a narrow range of W values that lead to the formation of a contact angle, as opposed to full wetting or dewetting. The present plots agree qualitatively with those determined by Giovambattista *et al.* [33] for the influence of the polarity of hydroxylated silica surfaces on the contact angle formed with water.

5 Computing performance

The scalability of the ls1/mardyn program was measured on the *cacau* supercomputer for typical simulation scenarios involving methane, represented by the TSLJ fluid, as well as graphite, modeled by a version of the Tersoff [30] potential that was rescaled to compensate for the bond length deviation found by Kelires [31]. MPI paralleliza-

tion was applied according to a spatial domain decomposition scheme with equally sized cuboid subdomains and a cartesian topology based on linked cells [24].

Often the best solution is an isotropic decomposition that minimizes the surface to volume ratio of the spatial subdomains. For the simulation of homogeneous systems, this approach is quite efficient. That is underlined by the weak and strong scaling behavior of ls1/mardyn for typical configurations, shown in Fig. 7 (left), in cases where supercritical methane ('fluid') at a density of 10 mol/l and solid graphite ('wall') were considered with a system size of up to 4,800,000 interaction sites, representing the same number of carbon atoms and methane molecules here. Graphite simulations, containing only carbon atoms, scale particularly well, due to a favorable relation of the delay produced by communication between processes to the concurrent parts, i.e., the actual intermolecular interaction computation, which is much more expensive for the Tersoff potential than the TSLJ potential.
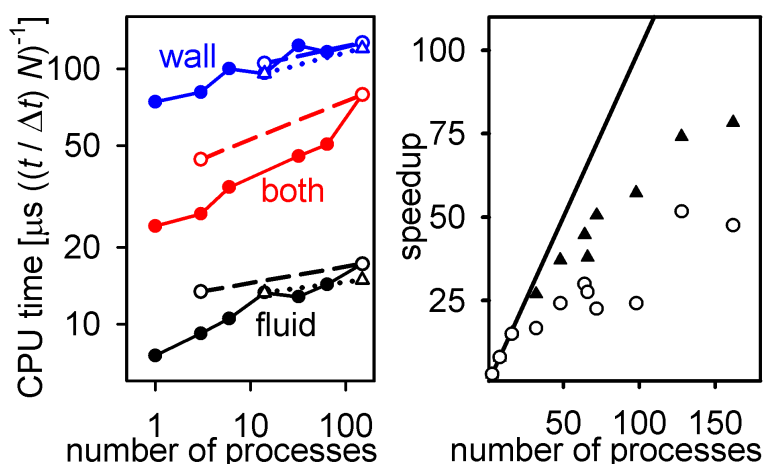

Fig. 7. Left: Total CPU time, i.e., execution time multiplied with the number of parallel processes, per time step and interaction site for weak scaling with 3,000 (dashed lines / circles) and 32,000 (dotted lines / triangles) interaction sites per process as well as strong scaling with 450,000 interaction sites (solid lines / bullets), using isotropic spatial domain decomposition. Right: speedup for a system of liquid methane between graphite walls with 650,000 interaction sites, where isotropic (circles) and channel geometry based (triangles) spatial domain decomposition was used; the solid line represents linear speedup.

The simulation of combined systems, containing both fluid and solid interaction sites, is better handled by a channel geometry based decomposition scheme, where an approximately equal portion of the wall and a part of the fluid is assigned to each process, cf. Fig. 7 (right). In the general case, where spatial non-uniformities do not match any cartesian grid, a flexible topology has to be used. An approach based on *k*-dimensional trees [34], implemented in a version of ls1/mardyn, showed clearly improved results with respect to the scaling of inhomogeneous systems.

6 A sterically accurate generic benzyl alcohol model

Benzyl alcohol (C_6H_5–CH_2OH) is widely used as a solvent for paints and inks. However, it is classified as a harmful substance (Xn) and should not be inhaled, nor used at high temperatures where it exhibits a high vapor pressure.

The basis for a new rigid molecular model of benzyl alcohol was determined by *ab initio* calculations with the GAMESS (US) quantum chemistry package [35], obtaining the equilibrium positions of the nuclei as illustrated in Fig. 8 as well as the quadrupole moment.

Further potential parameters were taken from accurate empirical molecular models for related fluids, leading to a sterically accurate generic model, cf. Tab. 1, that can be used as a starting point for parameter optimization. In particular, point charges as well as σ and ε parameters for the hydroxyl group were taken from the ethanol model of Schnabel *et al.* [36]. Moreover, the σ and ε values of the corresponding LJ interaction site of the Merker *et al.* [37] cyclohexanol model were used for the CH_2 group, while the LJ parameters for the CH and C centers were set according to the Huang *et al.* [38] models of benzene and phosgene, respectively.

VLE properties of the generic model were calculated using the ms2 program, leading to an overall satisfactory first approximation, considering that all a posteriori adjustments were absent. The vapor pressure is more accurate at high temperatures, cf. Fig. 9.
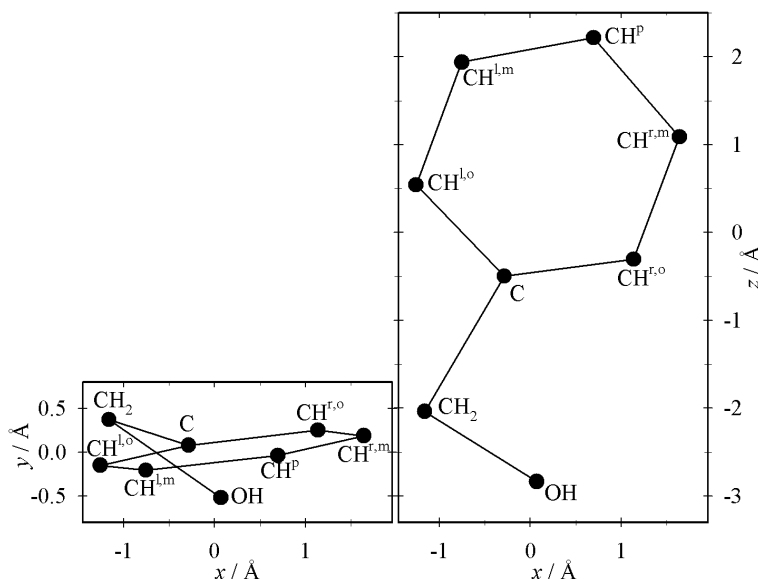

Fig. 8. Coordinates of the LJ sites for the present benzyl alcohol model.

Table 1. Coordinates and parameters of the LJ sites, and the point charges, and the point quadrupole for the present benzyl alcohol model. Bold characters indicate represented atoms.

Interaction site	x Å	y Å	z Å	σ Å	ε/k_B K	q e	Q DÅ
CH^p	0.695	-0.037	2.218	3.247	88.97		
CH^{l,m}	-0.753	-0.204	1.941	3.247	88.97		
CH^{r,m}	1.638	0.189	1.090	3.247	88.97		
CH^{l,o}	-1.255	-0.149	0.543	3.247	88.97		
CH^{r,o}	1.134	0.250	-0.304	3.247	88.97		
C	-0.285	0.080	-0.497	2.810	10.64		
CH$_2$	-1.160	0.372	-2.039	3.412	102.2	+0.2556	
OH	0.070	-0.516	-2.835	3.150	85.05	-0.6971	
O**H**	0.191	-1.430	-2.614			+0.4415	
Benzyl	0	0	0				2.534
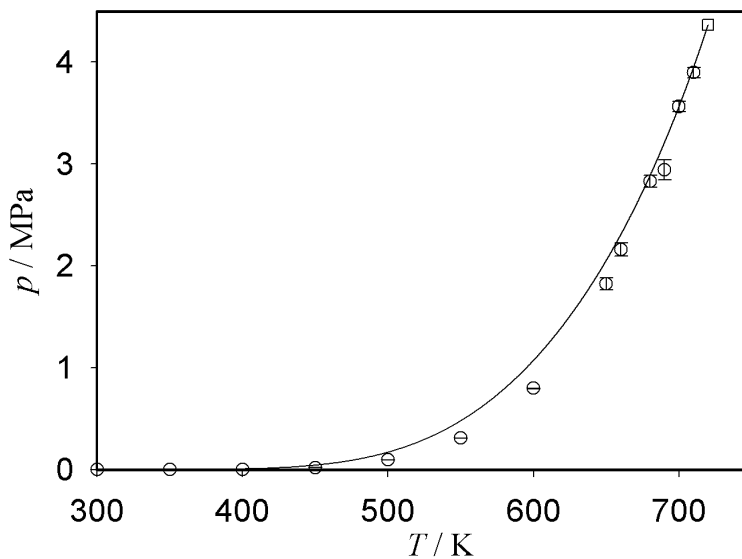
Fig. 9. Vapor pressure of benzyl alcohol according to a correlation [39] based on experiments (——) as well as present molecular simulation data (○).

7 Conclusion

The intermolecular interaction of small hydrogen bonding molecules like mono- and dimethylamine can be described by simple LJ based united-atom molecular models with point charges. Such computationally efficient models were applied to binary mixtures with non-hydrogen bonding components regarding VLE properties. Accurate predictions, covering a broad range of temperatures and compositions, were

obtained, regardless whether the state independent binary interaction parameter was adjusted to Henry's law constant or vapor pressure.

For a two-center LJ plus quadrupole model of carbon dioxide, a comparison of cluster criteria with the purpose of accurately detecting the vapor-liquid phase boundary gave overall support to the geometric mean density criterion applied to the sphere consisting of a molecule and its two nearest neighbours. The Stillinger criterion was found to be particularly adequate at low temperatures. For the TSLJ fluid, the contact angle formed between the vapor-liquid interface and a wall was determined by canonical ensemble MD simulation while the mangitude of the dispersive fluid-wall interaction was varied. Over the whole temperature range between triple point and critical point, the contact angle dependence on the fluid-wall dispersive energy obeys a simple symmetry law. The scalability of the ls1/mardyn program was assessed and found to be acceptable. MD simulations of methane confined between graphite walls with up to 4,800,000 interaction sites, i.e., carbon atoms and methane molecules, were conducted to demonstrate the viability of the program.

A sterically realistic model for benzyl alcohol was presented, showing within the framework of Lennard-Jones sites with point polarities and electric point charges that the generic molecular modeling approach can lead to a good starting point for parameter optimization with respect to VLE properties such as the vapor pressure.

References

1. Schnabel, T., Vrabec, J. & Hasse, H. Unlike Lennard-Jones parameters for vapor-liquid equilibria. *J. Mol. Liq.* **130**, 170–178 (2007).
2. Vrabec, J., Stoll, J. & Hasse, H. Molecular models of unlike interactions in fluid mixtures. *Mol. Sim.* **31**, 215–221 (2005).
3. Ungerer, P., Nieto-Draghi, C., Rousseau, B., Ahunbay, G. & Lachet, V. Molecular simulation of the thermophysical properties of fluids: From understanding toward quantitative predictions. *J. Mol. Liq.* **134**, 71–89 (2007).
4. Schnabel, T., Vrabec, J. & Hasse, H. Molecular simulation study of hydrogen bonding mixtures and new molecular models for mono- and dimethylamine. *Fluid Phase Equilib.* **263**, 144–159 (2008).
5. Vrabec, J., Huang, Y.-L. & Hasse, H. Molecular models for 267 binary mixtures validated by vapor-liquid equilibria: A systematic approach. *Fluid Phase Equilib.* **279**, 120–135 (2009).
6. Vishnyakov, A., Ravikovitch, P. I. & Neimark, A. V. Molecular level models for CO_2 sorption in nanopores. *Langmuir* **15**, 8736–8742 (1999).

7. Werder, T., Walter, J. H., Jaffe, R. L., Halicioglu, T. & Koumoutsakos, P. On the water-carbon interaction for use in molecular dynamics simulations of graphite and carbon nanotubes. *J. Phys. Chem. B* **107**, 1345–1352 (2003).

8. Teletzke, G. F., Scriven, L. E. & Davis, H. T. Wetting transitions. II. First order or second order? *J. Chem. Phys.* **78**, 1431–1439 (1982).

9. Wedekind, J. & Reguera, D. What is the best definition of a liquid cluster at the molecular scale? *J. Chem. Phys.* **127**, 154516 (2007).

10. Schnabel, T., Cortada, M., Vrabec, J., Lago, S. & Hasse, H. Molecular model for formic acid adjusted to vapor-liquid equilibria. *Chem. Phys. Lett.* **435**, 268–272 (2007).

11. Hong, J. H., Malone, P. V., Jett, M. D. & Kobayashi, R. The measurement and interpretation of the fluid-phase equilibria of a normal fluid in a hydrogen bonding solvent: the methane-methanol system. *Fluid Phase Equilib.* **38**, 83–96 (1987).

12. Yarym-Agaev, N. I., Sinyavskaya, R. P., Koliushko, I. I. & Levinton, L. Y. *J. Appl. Chem. USSR* **58**, 154–157 (1985).

13. Levi, M. G. *Gazzetta Chimica Italiana* **31**, 513–541 (1901).

14. McDaniel, A. S. The absorption of hydrocarbon gases by nonaqueous liquids. *J. Phys. Chem.* **15**, 587–610 (1911).

15. Bezdel, L. S. & Teodorovich, V. P. *Gazovaya Prom.* **8**, 38–43 (1958).

16. Boyer, F. L. & Bircher, L. J. The solubility of nitrogen, argon, methane, ethylene and ethane in normal primary alcohols. *J. Phys. Chem.* **64**, 1330–1331 (1960).

17. Lannung, A. & Gjaldback, J. *Acta Chem. Scand.* **14**, 1124–1128 (1960).

18. Shenderei, E., Zelvenskii, Y. & Ivanovskii, F. *Gazovaya Prom.* **6**, 42–45 (1961).

19. Tokunaga, J. & Kawai, M. Solubilities of methane in methanol-water and ethanol-water solutions. *J. Chem. Eng. Jap.* **8**, 326–327 (1975).

20. Makranczy, J., Rusz, L. & Balog-Megyery, K. *Hung. J. Ind. Chem.* **7**, 41–46 (1979).

21. Tkaczuk, P. Experimentelle Bestimmung der Gaslöslichkeit von Methan in Ketonen und Vergleich mit vorausberechneten Ergebnissen. Tech. Rep., Technische Universität Dortmund (1986).

22. Bo, S., Battino, R. & Wilhelm, E. Solubility of gases in liquids. 19. solubility of He, Ne, Ar, Kr, Xe, N_2, O_2, CH_4, CF_4, and SF_6 in normal 1-alkanols n-$C_\ell H_{2\ell}OH$ ($1 \leq \ell \leq 11$) at 298.15 K. *J. Chem. Eng. Data* **38**, 611–616 (1993).

23. Knapp, H., Yang, X. & Zhang, Z. Vapor-liquid equilibria in ternary mixtures containing nitrogen, methane, ethane and carbondioxide at low temperatures and high pressures. *Fluid Phase Equilib.* **54**, 1–18 (1990).

24. Bernreuther, M. & Vrabec, J. Molecular simulation of fluids with short range potentials. In Resch, M., Bönisch, T., Benkert, K., Furui, T. & Bez, W. (eds.) *High Performance Computing on Vector Systems*, 187–195 (Springer, Heidelberg, 2006).

25. Vrabec, J., Stoll, J. & Hasse, H. A set of molecular models for symmetric quadrupolar fluids. *J. Phys. Chem. B* **105**, 12126–12133 (2001).

26. Stillinger, F. H. Rigorous basis of the Frenkel-Band theory of association equilibrium. *J. Chem. Phys.* **38**, 1486–1494 (1963).

27. Ten Wolde, P. R. & Frenkel, D. Computer simulation study of gas-liquid nucleation in a Lennard-Jones system. *J. Chem. Phys.* **109**, 9901–9918 (1998).

28. Allen, M. P. & Tildesley, D. J. *Computer Simulation of Liquids* (Clarendon, Oxford, 1987).

29. Vrabec, J., Kedia, G. K., Fuchs, G. & Hasse, H. Comprehensive study on vapour-liquid coexistence of the truncated and shifted Lennard-Jones fluid including planar and spherical interface properties. *Mol. Phys.* **104**, 1509–1527 (2006).

30. Tersoff, J. Empiric interatomic potential for carbon, with applications to amorphous carbon. *Phys. Rev. Lett.* **61**, 2879–2882 (1988).

31. Kelires, P. C. Structural properties and energetics of amorphous forms of carbon. *Phys. Rev. B* **47**, 1829–1839 (1993).

32. Dong, T., Yang, Z. & Wu, H. Molecular simulations of R114b boiling flow in micro/nano channel: Interfacial phenomena. *Energ. Conv. Manag.* **47**, 2178–2191 (2006).

33. Giovambattista, N., Debenedetti, P. G. & Rossky, P. J. Effect of surface polarity on water contact angle and interfacial hydration structure. *J. Phys. Chem. B* **111**, 9581–9587 (2007).

34. Bentley, J. L. Multidimensional binary search trees used for associative searching. *CACM* **18**, 509–517 (1975).

35. Schmidt, M. W. *et al.* General atomic and molecular electronic structure system. *J. Comp. Chem.* **14**, 1347–1363 (1993).

36. Schnabel, T., Vrabec, J. & Hasse, H. Henry's law constants of methane, nitrogen, oxygen and carbon dioxide in ethanol from 273 to 498 k: Prediction from molecular simulation. *Fluid Phase Equilib.* **233**, 134–143 (2005). See also Fluid Phase Equilib. 236: 272 (2005) and 239: 125–126 (2006).

37. Merker, T., Guevara-Carrión, G., Vrabec, J. & Hasse, H. Molecular modeling of hydrogen bonding fluids: New cyclohexanol model and transport properties of short monohydric alcohols. In Nagel, W. E., Kröner, D. B. & Resch, M. M. (eds.) *High Performance Computing in Science and Engineering '08, Transactions of the High Performance Computing Center, Stuttgart*, 529–541 (Springer, Heidelberg, 2009).

38. Huang, Y.-L., Hasse, H. & Vrabec, J. Molecular modeling of industrially relevant aromatic fluids. In preparation.

39. Rowley, R. L. *et al.* *DIPPR R Data Compilation of Pure Compound Properties* (AIChE, New York, 2006).